Biomaterials Science

ROYAL SOCIETY OF CHEMISTRY

PAPER

View Article Online
View Journal | View Issue

Cite this: *Biomater. Sci.*, 2024, **12**, 5023

Structure–function relationship of phase-separated liposomes containing diacylglycerol analogues†

Panagiota Papadopoulou, ‡[a] Gabriela Arias-Alpizar, ‡[b] Pim Weeda,[a] Thijs Poppe,[a] Niels van Klaveren,[a] Tomas Slíva,[a] Dennis Aschmann,[a] Winant van Os,[a] Yun Zhang,[a] Mohammad-Amin Moradi,[c] Nico Sommerdijk,[d,e] Frederick Campbell[a] and Alexander Kros *[a]

The composition and morphology of lipid-based nanoparticles can influence their overall *in vivo* behavior. Previously, we demonstrated that phase separation in liposomes composed of DSPC and a diacylglycerol lipid analogue (DOaG) drives the *in vivo* biodistribution towards a specific subset of endothelial cells in zebrafish embryos. In the absence of traditional targeting functionalities (*e.g.*, antibodies, ligands), this selectivity is mediated solely by the unique liposome morphology and composition, characterized by a DOaG-rich lipid droplet within the DSPC-rich phospholipid bilayer. The phase separation is induced due to the geometry of DOaG lipid and its ability to create non-bilayer phases in lipid membranes. To investigate the underlying principles of phase separation and to optimize the liposome colloidal stability, we performed a structure–function relationship study by synthesizing a library of DOaG analogues with varying molecular properties, such as the number, length and *sn*-position of the acyl chains, as well as the degree of saturation or carbonyl substituents. We assessed the ability of these lipid analogues to assemble into phase-separated liposomes and studied their morphology, colloidal stability, and *in vivo* biodistribution in zebrafish embryos. We found that analogues containing unsaturated, medium length (C16–C18) fatty acids were required to obtain colloidally stable, phase-separated liposomes with cell-specific biodistribution patterns. Moreover, we observed that using the pure DOaG isomer, with acyl chains at the *sn*-1,3 positions, leads to more colloidally stable liposomes than when a mixture of *sn*-1,2 and *sn*-1,3 isomers is used. Similarly, we observed that incorporating a DOaG analogue with fatty tails shorter than DSPC, as well as PEGylation, endows liposomes with long term stability while retaining cell-selective biodistribution. Diacylglycerols are known to promote fusion, lipid polymorphism, signaling and protein recruitment on lipid membranes. In this study, we showed that diacylglycerol derivatives can induce phase separation in liposomes, unlocking the potential for cell-specific targeting *in vivo*. We believe that these findings can be the foundation for future use of diacylglycerols in lipid-based nanomedicines and could lead to the development of novel targeted delivery strategies.

Received 13th June 2024,
Accepted 30th July 2024

DOI: 10.1039/d4bm00799a

rsc.li/biomaterials-science

[a]*Department of Supramolecular & Biomaterials Chemistry, Leiden Institute of Chemistry (LIC), Leiden University, P.O. Box 9502, 2300 RA Leiden, The Netherlands. E-mail: a.kros@chem.leidenuniv.nl*
[b]*Division of BioTherapeutics, Leiden Academic Centre for Drug Research, Leiden University, P.O. Box 9502, 2300 RA Leiden, The Netherlands*
[c]*Materials and Interface Chemistry, Department of Chemical Engineering and Chemistry, Eindhoven University of Technology, P.O. Box 513, 5600 MB Eindhoven, The Netherlands*
[d]*Electron Microscopy Center, Radboud Technology Center Microscopy, Radboud University Medical Center, Nijmegen, The Netherlands*
[e]*Department of Biochemistry, Radboud Institute of Molecular Life Sciences, Radboud University Medical Center, Nijmegen, The Netherlands*

†Electronic supplementary information (ESI) available. See DOI: **https://doi.org/10.1039/d4bm00799a**

‡These authors contributed equally.

Introduction

The composition and molecular properties of lipids used in lipid-based nanoparticles play a pivotal role in their overall *in vivo* behavior. Charge, geometry, and the degree of saturation, as well as a combination of different lipids and molar ratios, dictate lipid nanoparticle size, morphology, rigidity and surface chemistry. Upon *in vivo* administration, these physicochemical properties influence the protein corona formation, clearance, cell uptake and endocytic routes, thereby controlling the overall biodistribution of lipid-based nanoparticles.[1–4] However, the underlying principles are still only understood at the basic level, limiting the effective design of nanomedicines

with a high therapeutic efficacy. Whereas strong surface charge – either anionic or cationic – appears to lead to dominant interactions in the body,[5–10] the fate of neutral lipid nanoparticles appears more nuanced.[1,3,6,8] The geometry of individual lipids contributes to lipid polymorphism[11,12] and controls the morphological and physicochemical properties of lipid nanoparticles, which in turn determine the particle–protein interactions and *in vivo* fate.[13–16] Inverted conical lipids with bulky polar head groups result in assemblies with a positive curvature (*i.e.* micelles), while lipids with cylindrical geometry result in planar lamellar bilayers (*i.e.* liposomes).[11,17] Conical lipids with small polar headgroups increase the negative curvature of membranes providing fusogenic properties in lipid nanoparticles[11,18] and facilitate endosomal escape after endocytosis, a crucial event for drug and nucleic acid delivery.[13,19,20] Additionally, conical lipids can lead to non-bilayer phases *i.e.*, the inverse hexagonal phase.[17,21–26] One example of such lipids are diacylglycerols (DAGs).[27] DAGs are endogenous lipids found in the cell membrane – mainly after the hydrolysis of phosphatidylinositol – and activate enzymes such as Protein Kinase C (PKC) or phospholipase C, promoting the signaling cascade.[27] Lacking a phosphate group, DAGs are hydrophobic conical lipids which can occupy the interleaflet space of lamellar lipid membranes. Above a critical concentration in the bilayer, local accumulation of DAGs disrupts the lamellar properties of membranes and leads to phase separation and formation of lipid droplets buried within the phospholipid leaflet.[28–32] Recently, we demonstrated how DAG-induced phase separation can drive the *in vivo* targeting of mRNA-LNPs and liposomes to specific endothelial cell types in zebrafish embryos.[15,16] The liposome formulation (denoted as PAP3) consisting of an equimolar mixture of the saturated, naturally occurring phospholipid DSPC (1,2-distearyl-*sn-glycero*-3-phosphatidylcholine, T_m = 55 °C) and a synthetic DAG analogue, DOaG (2-hydroxy-3-oleamidopropyl-oleate, or dioleoylamidoglycerol), resulted in phase-separated liposomes bearing a single lipid droplet in each bilayer (Fig. 1a and b). Surprisingly, upon intravenous administration in zebrafish embryos, PAP3 liposomes selectively accumulated within brain endothelial cells (bECs) without the use of traditional targeting ligands (*e.g.*, antibodies, peptides) (Fig. 1c). The observed liposome recognition and accumulation in bECs was mediated by triglyceride lipase (TGL), which is highly present at the luminal surface of zebrafish bECs during development. Importantly, we showed that this process required the presence of the phase-separated droplet within the liposome bilayer, implying a preferential nanoparticle–protein communication due to the unique morphology and composition.[15,16] Additionally, we found that accumulation of DOaG within the DSPC leaflet induced lipid packing defects on the liposome surface, exposing the DOaG to the surrounding environment, a key factor for the specific interaction between the PAP3 liposomes and TGL.[16] As with DAGs, DOaG increases the distance between adjacent phospholipids, increasing the hydrophobicity and facilitating recognition and binding of TGL on the lipid membrane.[16,31,33]

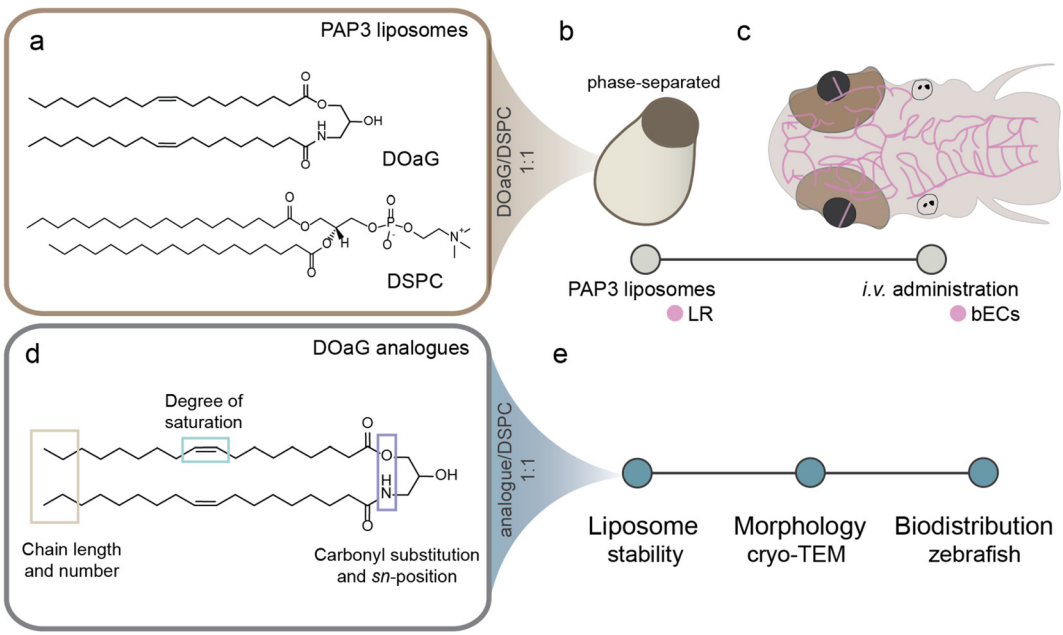

Fig. 1 Overview of phase-separated liposomes and the timeline of experiments. (a) Molecular structures of DOaG and DSPC. (b) Schematic of phase-separated liposomes containing DOaG and DSPC (1 : 1). (c) Schematic dorsal view of the zebrafish embryo head. Injected liposomes contained 0.2% mol DOPE-LR (1,2-dioleoyl-*sn-glycero*-3-phosphoethanolamine-*N*-[lissamine rhodamine B sulfonyl]) for visualization. (Brain) vasculature depicted in pink, the region in which liposomes selectively accumulate. (d) Molecular properties of DOaG which were altered to generate a library of DOaG analogues. (e) Overview of DOaG library assessment: liposomes were formulated from a 1 : 1 ratio of DSPC : analogue and the stability, morphology and biodistribution were assessed by DLS, cryo-TEM and confocal imaging of injected zebrafish embryos, respectively.

In this study, we designed a library of close DOaG analogues to probe how the exact molecular chemistry and structure of DOaG induce phase separation in liposomes and concomitant bEC targeting in embryonic zebrafish. The chain length, degree of saturation, number and *sn*-position of fatty acid chains, and carbonyl substituents on the backbone were varied to study the effect on lipid assembly and *in vivo* cell-specific targeting (Fig. 1d). Hence, molecular DOaG analogues were synthesized, mixed with DSPC (analogue/DSPC_1 : 1) and assembled into liposomes. The long-term stability and morphology of the resulting liposomes were characterized by dynamic light scattering (DLS) and cryo-transmission electron microscopy (cryo-TEM) respectively and their *in vivo* behavior was assessed in zebrafish embryos (Fig. 1e).

The chain length in DAGs, as well as the degree of saturation, has been previously observed to affect lipid packing, curvature, and activation of protein kinase C (PKC) in phospholipid bilayers.[32,34] Therefore, we hypothesize that DOaG variants with short chains will not be able to create high packing defects and be exposed to the surrounding environment, resulting therefore in an abolishment/reduction of the bEC targeting (less recognition by TGL). Additionally, since packing defects may affect colloidal stability, we hypothesize that DOaG variants with shorter chains may result in higher long-term stability and *vice versa*. Overall, we observed that DOaG analogues with unsaturated, medium length (C16–C18) fatty acid tails – when co-formulated with DSPC – can induce phase separation in colloidally stable liposome formulations, which leads to bEC specific biodistribution patterns in embryonic zebrafish. Monoacyl and triacyl glycerol analogues, as well as diacyl analogues with saturation, or shorter (C14) or longer fatty acid tails (C20–C24), either (i) cannot form liposomes, or (ii) phase separation exists only in a small fraction of the population, or (iii) the formulation cannot interact with bECs. Additionally, we show that the naturally occurring dioleoylglycerol (DOG) retains the properties of DOaG, proving the correlation of the well-studied DAGs in membranes with the DOaG-induced phase separation. Finally, we show that lipids with fatty acid tails substituting the *sn*-1,3 positions of the backbone result in liposomes with more favorable long-term stability than when the *sn*-1,2 positional isomer is also present in the formulation. Similarly, PAP3 liposomes could be stabilized by a small amount of DMPE-PEG2k (1,2-dimyristoyl-*sn-glycero*-3-phosphoethanolamine-*N*-[methoxy(polyethylene glycol)-2000]), or by replacing DOaG with the shorter (C16:1) analogue. This improved the long-term stability and ability to assemble liposomes in physiologically relevant buffers, which is particularly important for the translation towards nanomedicine formulations with high therapeutic efficacy.

Results

Molecular library of DOaG analogues

DOaG is a synthetic, amide-containing analogue of DOG (Fig. 2a and b). It is mainly isolated as a mixture of two positional isomers – something that also occurs in natural lipids – in which the two acyl chains substitute the *sn*-1,3 positions and *sn*-1,2 positions with a 8 : 2 ratio (Fig. S1†). To understand the influence of individual molecular properties of the DOaG lipid, a library of 12 analogues was created, maintaining the glycerol-like backbone in all newly synthesized lipids (Fig. 2b). Firstly, a series of changes in the chain length was generated, altering the monounsaturated fatty acid chains, from C14:1 to C24:1, resulting in lipids **1–5** (Fig. 2c and Fig. S2b, g.† Note: lipid **3** is DOaG). Subsequently, the degree of saturation was altered (Fig. 2d and Fig. S2c, g†), with either full saturation in both C18 tails, one saturated (lipid **6**) and one monounsaturated tail (lipid **7**) or with di-unsaturation in both tails (lipid **8**). Next, we generated lipids with only one, or three oleic chains and lipids with either two esters (naturally occurring DAG), or two amides (Fig. 2e, f and Fig. S2d, e, g,† lipids **9–12**). Finally, to assess the importance of the regioisomeric mixture of positional isomers, we synthesized the pure DOaG isomer with substitution on the *sn*-1,3 position (~95% pure), as a comparison of the mixture that has been studied so far (*sn*-1,3/80%, *sn*-1,2/20%) (lipid **21**, Fig. 2g and Fig. S2f, g†).

Chain length influences stability and bEC targeting

Liposomes containing an equimolar mixture of DSPC and the **C14:1** analogue (lipid **1**) were stable over a period of up to ~25 days, maintaining their hydrodynamic diameter below 200 nm albeit with the polydispersity increasing after 6 days (Fig. 3a). The majority (80%) of the liposomes revealed a phase-separated morphology (Fig. 3b) as quantified by cryo-TEM (Fig. S3a and d†). Interestingly, real-time biodistribution imaging in zebrafish suggested that these liposomes mostly accumulate in a subset of cells located in the tail region of the zebrafish embryo, named as scavenging endothelial cells[6] and in the zebrafish liver, but not in bECs despite their phase-separated morphology (Fig. 3c and Fig. S4a, b†). This finding supports the hypothesis that the C14:1 analogue might be too short to create high packing defects at the liposome membrane, resulting in less exposure to the surrounding environment and therefore no recognition by TGL and no bEC targeting. However, further experiments – possibly with the help of molecular dynamics simulations – need to be conducted to support this hypothesis. Liposomes assembled from the C16:1 analogue (**lipid 2**) were stable over a period of 30 days and monodisperse (Fig. 3d). Phase separation was also observed in these liposomes, while the bilayers appeared less cornered (less flat) suggesting a more liquid disordered phase than the C14:1 containing liposomes (Fig. 3e and Fig. S3b†). This indicates that C16:1 analogues are able to mix with the DSPC-rich membranes more effectively due to a smaller chain length mismatch. Therefore, the membrane becomes more flexible, resulting in more spherical liposomes with less corners. Quantification indicated that the majority of liposomes (~90%) possessed a phase-separated morphology (Fig. S3d†). Liposomes containing the C16:1 variant were also able to target bECs (Fig. 3f and Fig. S4c, d†), similar to the original PAP3 liposomes[15] which contain **C18:1** chains (DOaG, **lipid 3**

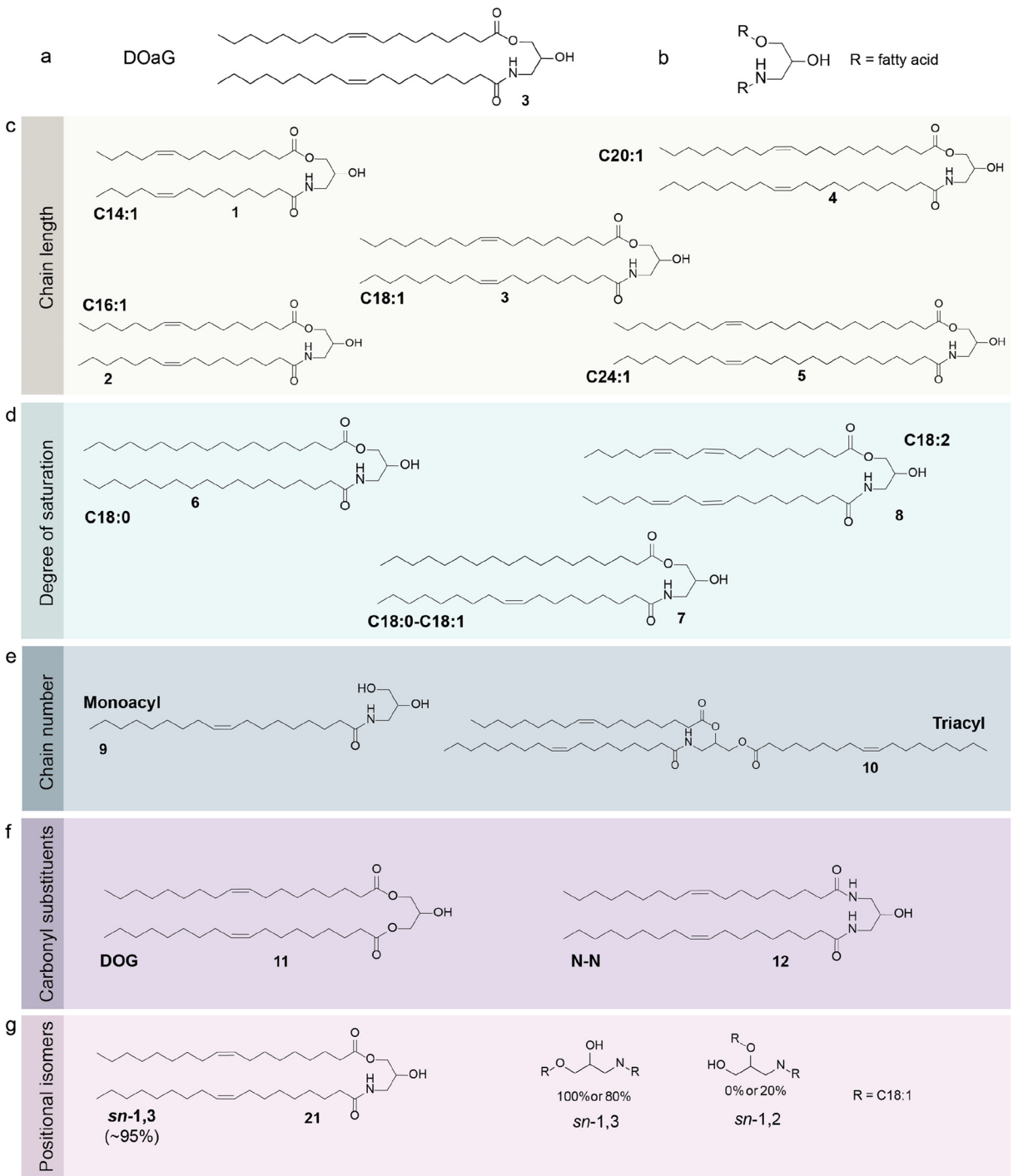

Fig. 2 Library of DOaG variants used in this study. (a) Molecular structure of DOaG lipid. (b) DOaG glycerol-like backbone. DOaG analogues with varying: (c) chain length, (d) degree of saturation, (e) number of acyl chains, (f) carbonyl substituents of the glycerol-like backbone and (g) *sn*-position of acyl chain substitution. All lipids exist as a regioisomeric mixture of *sn*-1,3 and *sn*-1,2 positional isomers (8 : 2 ratio), except for **7**, **9**, **10**, **12**, and **21**. Only the *sn*-1,3 isomer is shown for clarity.

in Fig. 2c) (compare Fig. 3f with Fig. 3i and Fig. S4e, f†). Extending the unsaturated chain length by 2 carbons (**C18:1**) decreased the stability of the resulting liposomes, as these were only stable and monodisperse for less than 7 days (Fig. 3g). The membrane of the phase-separated **C18:1** containing liposomes appeared more fluid as evidenced by the more spherical shape of the liposomes compared to the **C14:1** and **C16:1** variants (Fig. 3h and Fig. S3c†). Similar to **C16:1** containing liposomes, **C18:1** containing liposomes were predominantly phase-separated (Fig. S3d†). Further extension of the

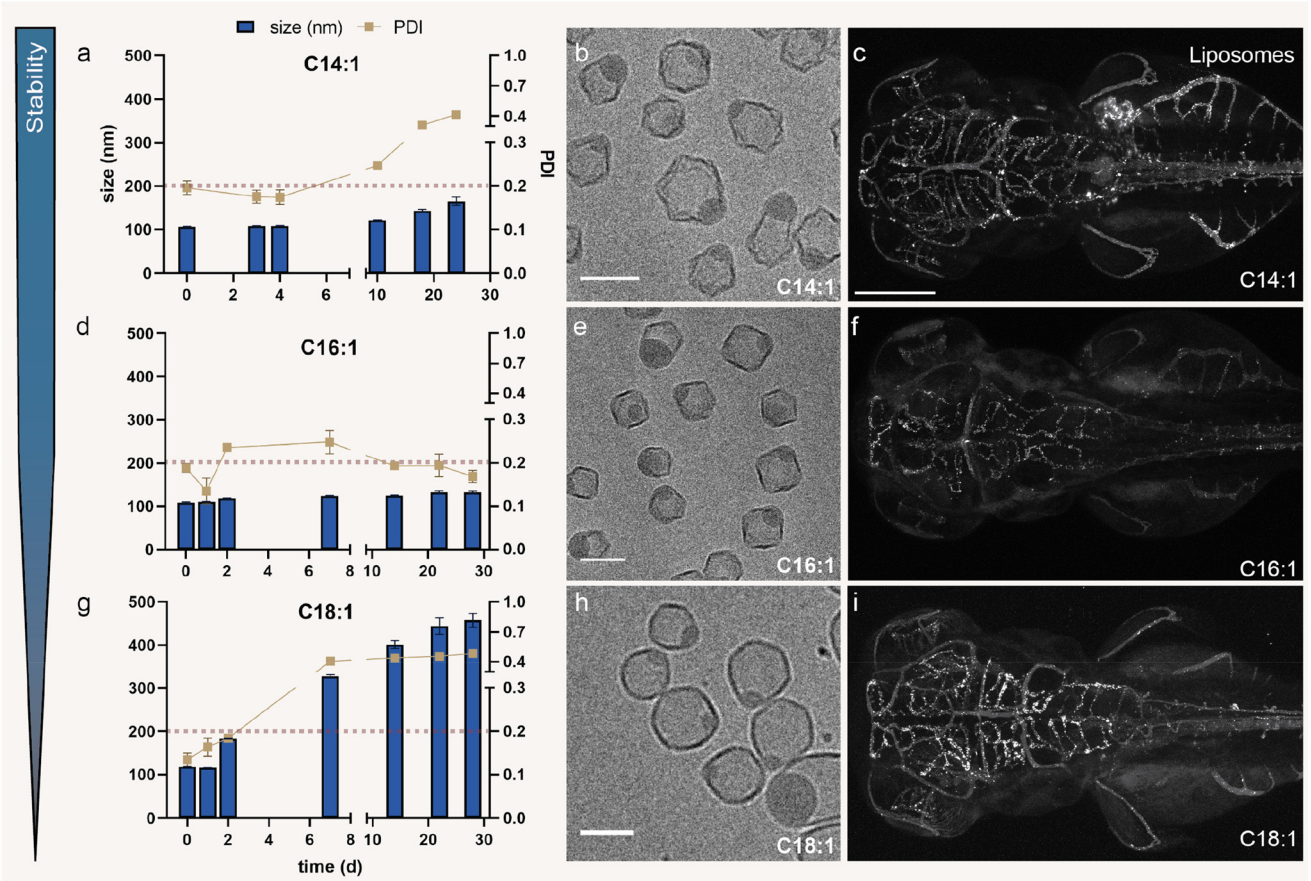

Fig. 3 Stability, morphology and biodistribution of liposomes consisting of DSPC and DOaG analogues as a function of chain length. (a) Size (nm) and polydispersity index (PDI) of liposomes consisting of DSPC and C14:1 variant over a period of ~30 days, (b) cryo-TEM image of liposomes consisting of DSPC and C14:1 variant (c) biodistribution of liposomes consisting of DSPC and C14:1 variant (grey) in a zebrafish embryo, in dorsal view (10× magnification), 1.5 hours post injection (hpi) at 78 days post fertilization (dpf). (d) Size (nm) and PDI of liposomes consisting of DSPC and C16:1 variant over a period of ~30 days, (e) cryo-TEM image of liposomes consisting of DSPC and C16:1 variant, (f) biodistribution of liposomes consisting of DSPC and C16:1 variant (grey) in a zebrafish embryo, in dorsal view (10× magnification), 1.5 hpi at 78 dpf. (g) Size (nm) and PDI of liposomes consisting of DSPC and C18:1 variant (PAP3 liposomes) over a period of ~30 days, (h) cryo-TEM image of liposomes consisting of DSPC and C18:1 variant (PAP3 liposomes), (i) biodistribution of liposomes consisting of DSPC and C18:1 variant (PAP3 liposomes) (grey) in a zebrafish embryo, in dorsal view (10× magnification), 1.5 hpi at 78 dpf. Liposomes consisting of 1 : 1 DSPC/analogue, total lipid concentration 5 mM containing 0.2 mol% DOPE-LR (grey scale fluorescence indicates the LR signal only, representing liposome distribution). Zebrafish embryo is a Tg(*kdrl* : eGFP) (see Fig. S4† for the eGFP signal). Scale bars: 200 μm for zebrafish and 100 nm for cryo-TEM images. Dynamic light scattering (DLS) was used to obtain data in (a), (d) and (g). The red dashed line in (a), (d) and (g) indicates the threshold of size and PDI relevant for *in vivo* use. Cryo-TEM imaging at d = 0.

acyl chains to **C20:1** DOaG analogue (**lipid 4**) resulted in aggregation after only ~6 h (Fig. S5a†), while the **C24:1** variant (**lipid 5**) did not assemble into liposomes at all (Fig. S5b†). These findings, as well as the instability of the **C18:1**-containing formulation (PAP3), indicate that liposomes progressively aggregate by increasing the fatty acid chain length, when mixed with DSPC. This supports previous findings which show that DOaG is exposed to the surrounding environment due to large hydrophobic packing defects induced in the membrane, due to phase separation.[16] Hence, the longer the fatty acid tail of the variant, the more the variant is exposed to the surroundings and therefore the shorter the stability of the overall assembly and *vice versa*. We have previously reported that packing defects on PAP3 liposomes are a key factor for liposome recognition by TGLs,[16] which in turn influences liposome uptake *in vivo*.[15]

Liposomes which contain the shorter chain (C14:1) analogue did not target bECs but are phase-separated. A possible explanation for this observation is that packing defects on these liposomal membranes are lower throughout. C14:1 lipids may possibly be more buried within the leaflet and less exposed on the liposome surface, due to their shorter chains and high mismatch with DSPC; therefore the liposome surface is less favorable for protein recruitment. Increasing the chain length by two carbons (C16:1 analogue) is already enough to create liposomes that target bECs, indicating again the starting point of exposure and accessibility of the lipid. This in turn indicates that C16:1 creates fewer packing defects than the longer C18:1 (DOaG) lipid and so forth. This hypothesis is supported by the colloidal stability studies, in which C16:1 containing liposomes are shown to be more stable and less prone to aggregation than the C18:1 containing liposomes. Since

liposomes with >C18 chains do not form stable formulations, C16:1 and C18:1 lipids seem to be the "sweet spot" for phase separation, liposome stability and bEC targeting.

Unsaturated analogues favor liposome formation and phase separation

We next assessed the effect that unsaturation in DOaG analogues has on the liposome assembly, by synthesizing a fully saturated variant (**C18:0**, **lipid 6**). This analogue could not be formulated into liposomes with DSPC as a co-formulant (Fig. S6a†). The intermediate lipid analogue C18:0–C18:1 (**lipid 7**) was also unable to assemble into stable liposomes (Fig. S6b†). This confirmed that both acyl chains must be unsaturated in order to assemble into stable phase-separated liposomes with DSPC. Indeed, as with DOaG, similar results were obtained with the DOaG analogue with two (conjugated) double bonds in each fatty acid tail (**C18:2**, **lipid 8**). Liposomes made of DSPC/C18:2 (1 : 1) were stable for at least 30 days, albeit with a moderate PDI (Fig. 4a). Cryo-TEM analysis showed that these liposomes were predominantly phase-separated (Fig. 4b and Fig. S7a, e†), but the bilayers appeared to be more in the gel-phase, as evidenced by cornered/flat membranes. The double unsaturation per acyl chain has a strong influence on the lipid's geometry and we assume the packing on this lipid within the DSPC leaflet might be more compact and completely de-mixed from DSPC, resulting in a gel-phase for the bilayer. Liposomes containing **C18:2** were able to target bECs in zebrafish embryos (Fig. 4c and Fig. S9a, b†). In conclusion, equimolar mixtures of unsaturated DOaG analogues and DSPC assemble into phase-separated liposomes, which in turn are able to selectively target bECs *in vivo*.

Influence of chain number and amide in the glycerol-like backbone

Next, we investigated how essential the number of acyl chains per glycerol is for phase separation. Monoacylglycerols have been studied before for their ability to form inverse hexagonal and (inverse) cubic liquid crystalline phases.[23,24] However, a liposome formulation with (1 : 1) DSPC and a **monoacyl** variant (**lipid 9**) formed liposomes that were highly unstable, as evidenced by the rapid size increase within ~6 h (Fig. S6d†). The **triacyl** variant (**lipid 10**), formulated with DSPC, formed liposomes that were stable for at least 30 days (Fig. 4d). Interestingly, these liposomes were predominantly lamellar in morphology (~80%), with some solid particles (~2%) and only a small fraction (~5%) which revealed a phase-separated morphology (Fig. 4e and Fig. S7b, e†). As a result, the majority of injected liposomes in zebrafish did not accumulate in the brain endothelium (Fig. 4f and Fig. S9c, d†). Only a minor fraction was able to target bECs, which might be explained by the fraction of phase-separated liposomes in the formulation. To assess the influence of the ester and amide functionalities of DOaG on phase separation and *in vivo* bEC targeting, we synthesized the naturally occurring dioleoylglycerol (**DOG**, **lipid 11**). Liposomes containing **DOG** were stable in size and with acceptable PDI values for a period of 20 days (Fig. 4g). Similar to **PAP3** liposomes, the **DOG** containing-liposomes revealed a phase-separated morphology (Fig. 4h and Fig. S7c†), albeit for only ~55% of all liposomes (Fig. S7e†). DOG/DSPC liposomes also targeted bECs (Fig. 4i). Interestingly, the lipid analogue with two amides (coded **N–N**, **lipid 12**) could not be formulated into stable liposomes (Fig. S6c†). A possible explanation may be an additional hydrogen bond due to the introduction of the extra amide, thereby negatively influencing lipid assembly into defined nanoparticles.

Sn-Position in fatty acid tails influences stability

Due to the chosen synthetic strategy, all previously discussed DOaG lipids (except for lipids 7, 9, 10 and 12) were a mixture of *sn*-1,2 and *sn*-1,3 isomers with a ~2 : 8 ratio. Therefore, we synthesized the *sn*-1,3 isomer in high purity (~95%, coded ***sn*-1,3**, **lipid 21**) and upon co-assembly with DSPC, stable liposomes were obtained for at least 30 days (Fig. 4j). In contrast, the original PAP3 liposomes, that contained the *sn*-1,3/*sn*-1,2 mixture, were only stable for 7 days (Fig. 3g). As expected, liposomes with *sn*-1,3 were phase-separated (Fig. 4k and Fig. S7d†), with only a small population (3.3%) having an unknown, highly structured liquid-crystalline phase (Fig. S7d, e and Fig. S8†), with a repeat distance of 4.85 nm as seen by Fast Fourier Transform (FFT) analysis. Biodistribution studies in zebrafish embryos revealed that liposomes containing this isomerically pure DOaG variant were also able to target bECs in a selective manner (Fig. 4l and Fig. S9g and h†).

C16:1 variant and pegylation improve long term stability

Despite their interesting morphology and selective *in vivo* behavior, PAP3 liposomes are not stable in physiologically isosmotic and isotonic buffers which contain saline (*i.e.*, phosphate buffered saline [PBS]). This is particularly important for the efficient applicability of these liposomal formulations towards nanomedicine. PAP3 liposomes formulated in water are stable for 7 days; however in PBS rapid aggregation is observed (Fig. 5a and b). This is likely due to the lack of ability of membranes which contain DAGs to coordinate sodium ions, as described in a previous study;[35] and although formulating liposomes containing the pure ***sn*-1,3** DOaG variant (*i.e.*, excluding the *sn*-1,2 isomer) improves the overall stability of PAP3 liposomes, it does not improve their stability in PBS (Fig. S10†). Interestingly, when co-formulated with DSPC, the shorter (**C16:1**) lipid variant could formulate stable phase-separated liposomes in PBS, with colloidal stability for at least 30 days and with improved PDI values (Fig. 5a and d). This supports our hypothesis that **C16:1** lipids are less exposed to the aqueous surroundings than DOaG, leading to less membrane instability and aggregation. Alternatively, a low percentage of PEGylated lipid also increased the stability of PAP3 liposomes, while retaining the morphology and bEC targeting. Previously, addition of 5% mol of DSPE-PEG2k-(1,2-distearoyl-*sn-glycero*-3-phosphoethanolamine-*N*-[amino(polyethyleneglycol)-2000]) in PAP3 was observed to abolish the bEC targeting.[15] Addition of only 1% mol of DMPE-PEG2k however showed to be optimal, keeping the *in vivo* bEC targeting while also improving liposo-

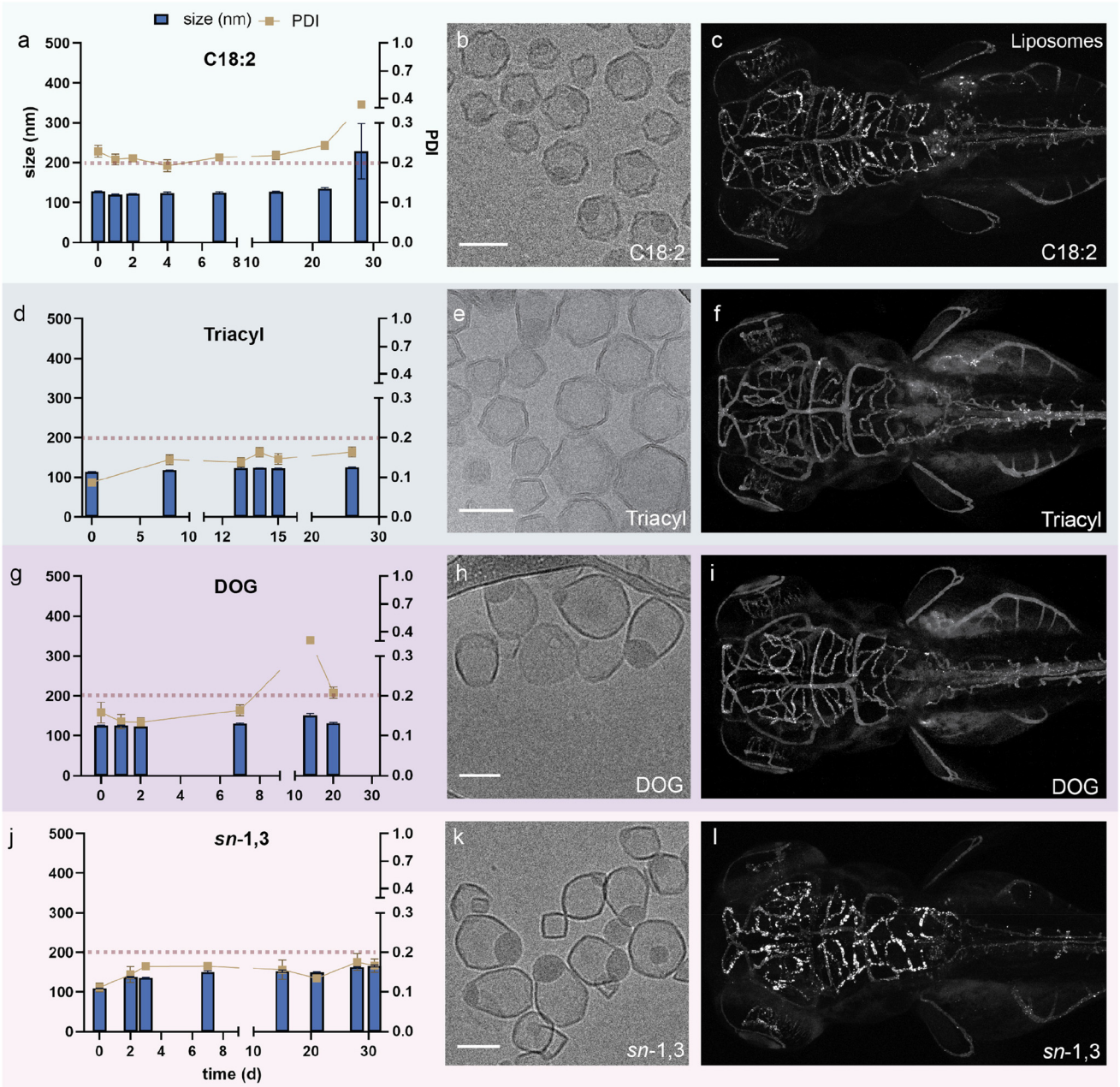

Fig. 4 Stability, morphology and *in vivo* behavior of liposomes consisting of DSPC and DOaG analogues as a function of saturation, number of fatty acid tails, carbonyl substitution or *sn*-position substitution. (a) Size (nm) and PDI of liposomes consisting of DSPC and C18:2 variant over a period of ~30 days, (b) cryo-TEM image of liposomes consisting of DSPC and C18:2 variant, (c) biodistribution of liposomes consisting of DSPC and C18:2 variant (grey) in a zebrafish embryo, in dorsal view (10× magnification), 1.5 hpi at 78 dpf. (d) Size (nm) and PDI of liposomes consisting of DSPC and triacyl variant over a period of ~30 days, (e) cryo-TEM image of liposomes consisting of DSPC and triacyl variant, (f) biodistribution of liposomes consisting of DSPC and triacyl variant (grey) in a zebrafish embryo in dorsal view (10× magnification), 1.5 hpi at 78 dpf. (g) Size (nm) and PDI of liposomes consisting of DSPC and DOG variant over a period of 20 days, (h) cryo-TEM image of liposomes consisting of DSPC and DOG variant, (i) biodistribution of liposomes consisting of DSPC and DOG variant (grey) in a zebrafish embryo, in dorsal view (10× magnification), 1.5 hpi at 78 dpf. (j) Size (nm) and PDI of liposomes consisting of DSPC and *sn*-1,3 variant over a period of ~30 days, (k) cryo-TEM image of liposomes consisting of DSPC and *sn*-1,3 variant, (l) biodistribution of liposomes consisting of DSPC and *sn*-1,3 variant (grey) in a zebrafish embryo, in dorsal view (10× magnification), 1.5 hpi at 78 dpf. Liposomes consisting of 1 : 1 DSPC/analogue, total lipid concentration 5 mM containing 0.2 mol% DOPE-LR (grey scale fluorescence indicates the LR signal only, representing liposome distribution). Zebrafish embryo is a Tg(*kdrl* : eGFP) (see Fig. S9† for the eGFP signal). Scale bars: 200 μm for zebrafish and 100 nm for cryo-TEM images. DLS was used to obtain data in (a), (d), (g) and (j). The red dashed line in (a), (d), (g) and (j) indicates the threshold of size and PDI relevant for *in vivo* use. Cryo-TEM imaging at $d = 0$.

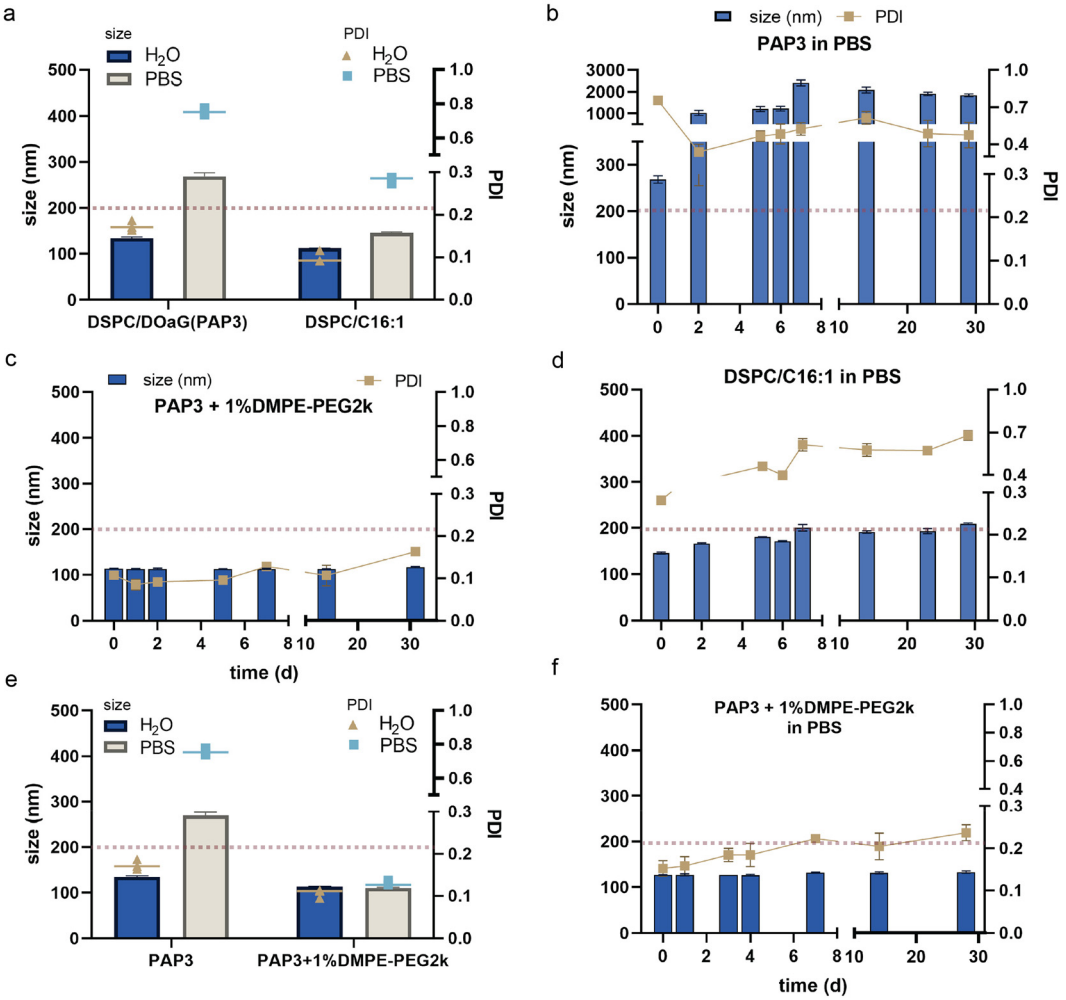

Fig. 5 Optimization and stability studies of PAP3 liposomes. (a) Size (nm) and PDI of PAP3 liposomes (DSPC/DOaG) or DSPC/C16:1 liposomes, formulated in ddH_2O or PBS. (b) Size (nm) and PDI of PAP3 liposomes formulated in PBS over a period of ~30 days. (c) Size (nm) and PDI of PAP3 liposomes coated with 1% mol DMPE-PEG2k formulated ddH_2O over a period of ~30 days. (d) Size (nm) and PDI of DSPC/C16:1 liposomes formulated in PBS over a period of ~30 days. (e) Size (nm) and PDI of PAP3 liposomes or PAP3 liposomes coated with 1% mol DMPE-PEG2k, formulated in ddH_2O or PBS. (f) Size (nm) and PDI of PAP3 liposomes coated with 1% mol DMPE-PEG2k formulated in PBS over a period of ~30 days. DLS was used to obtain the data depicted in this figure. The red dashed line indicates the threshold of size and PDI relevant for *in vivo* use.

mal stability (Fig. 5c). PAP3 liposomes with 1% mol DMPE-PEG are phase-separated (Fig. S11†) and target bECs in zebrafish embryos (Fig. S12†). Importantly, when formulated in PBS, the stability of PAP3 liposomes incorporating 1% mol of DMPE-PEG2k was improved even further than the **C16:1** variant (Fig. 5e and f). The information obtained by this effort to optimize phase-separated liposomes can be the basis for future developments, or use of DAGs and DAG analogues in lipid-based formulations.

Saturation in phospholipid co-formulant is important for phase separation

It is important to mention that liposomes with DOaG and the fluid DOPC (1,2-dioleoyl-*sn-glycero*-3-phosphocholine) as a co-formulant, instead of DSPC, do not formulate phase-separated liposomes and do not target bECs.[15] It was therefore interesting to assess the significance of saturated DSPC in the phase-separated liposomes. At room temperature, DSPC is a rigid phospholipid (T_m 55 °C) that prefers flat orientations and therefore does not favor curvature *i.e.*, spherical liposomes.[36] PAP3 liposomes are formed (above the T_m of all lipids, *i.e.*, 65 °C) and slowly reach room temperature, in which DSPC is in the gel-phase. We hypothesized that the gel-phase of DSPC is an important factor that induces phase separation. Indeed, cryo-TEM imaging at 45 °C < T < 65 °C reveals that ~50% of liposomes are in a fluid phase and non-phase separated, indicating full mixing of lipids (Fig. S13†). Therefore, phase separation seems to be induced after DSPC is in the gel-phase (<55 °C).

Discussion

In this study, we investigate the molecular details of DOaG, a DAG lipid analogue which – when co-formulated with DSPC –

leads to phase-separated liposomes able to target endothelial cell subsets *in vivo* and preferentially interact with TGLs *in vivo* and *in vitro*.[15,16] Through our structure–activity relationship screening we are able to show the narrow window of *in vivo* activity of phase-separated liposomes consisting of medium (C16–C18), unsaturated diacylglycerol analogues. All DAG analogues are summarized in Fig. 6, depicting the relationship between their chemical character, stability, morphology and *in vivo* fate of resulting liposomes. Briefly, we find that there is increasing instability in the liposome system, directly proportional to the DOaG chain length and the degree of saturation. Additionally, we show that monoacylglycerol or triacylglycerol counterparts do not result in liposomes with bEC specific behavior. Therefore, diacylglycerol analogues are the only molecules with the ability to phase-separate in membranes and result in liposomes targeting bECs in zebrafish embryos. Importantly, we show that the naturally occurring DAG equivalent has the same ability to form phase-separated liposomes (although in a lower percentage within the liposome population) and target bECs in zebrafish embryos. This gives strength to the basis of our background knowledge for the DOaG lipid, as it correlates with supporting previous studies of DAG properties in lipid membranes.[27,28,31,37]

Interestingly, we find phase-separated liposomes that do not target bECs (*i.e.*, **C14:1**). We theorize that lipid droplets may not be the only liposome part responsible for bEC targeting, but also all parts of the bilayer which have packing defects, exposing the DOaG analogue. Excess **C14:1** accumulates in the lipid droplet – which may indeed have high packing defects – but other parts of the bilayer may be unaffected due to its shorter chains. Liposomes therefore with only a fraction of their bilayer being defective may not have the same chance to expose DOaG analogues and be recognized and taken up by bECs, compared to liposomes with high packing defects throughout the bilayer (*i.e.*, **C16:1**, **C18:1**). Molecular dynamic simulations need to be conducted to support this hypothesis.

Additionally, we observe better long-term stability of liposomes containing the pure *sn*-1,3 positional isomer. The importance and effect of pure lipid isomers on lipid nanoparticle properties has been recently reported[38,39] and is an aspect to be considered in their development. Next, we find that liposomes consisting of the **C16:1** variant are overall more stable in PBS than the **C18:1** counterpart (DOaG) and that PEGylation of PAP3 liposomes (1% mol DMPE-PEG2k) increases the long-term stability even further, while phase separation and bECs targeting are retained. While PEGylation is generally known to improve long-term stability of lipid-based nanoparticles, PEG lipids with short chains (C14), such as DMPE-PEG2k, have been observed to dissociate from the lipid membrane *in vivo*.[40] In this study, dissociation allows for the nanoparticle to exhibit the same biological profile as PAP3 liposomes, thereby preserving the desired biodistribution. Herein, we display a selection of DOaG analogues co-formulated with DSPC. Combinations of DOaG analogues, DAGs, and co-formulants are virtually endless, nevertheless out of the scope of this study. This work is an effort to comprehend the overall properties of a highly unusual liposome with a specific *in vivo* behavior. Lacking any 'active' targeting ligands, these liposomes depend solely on the composition and morphology which dictate the nano–bio interactions. Therefore, this compositionally simple system can offer new perspectives in the design of 'targeted' liposome formulations. This work also highlights the importance of lipid composition in lipid-based nanoparticles, as even the smallest molecular changes in lipid components can greatly affect their macromolecular assembly and *in vivo* behavior.

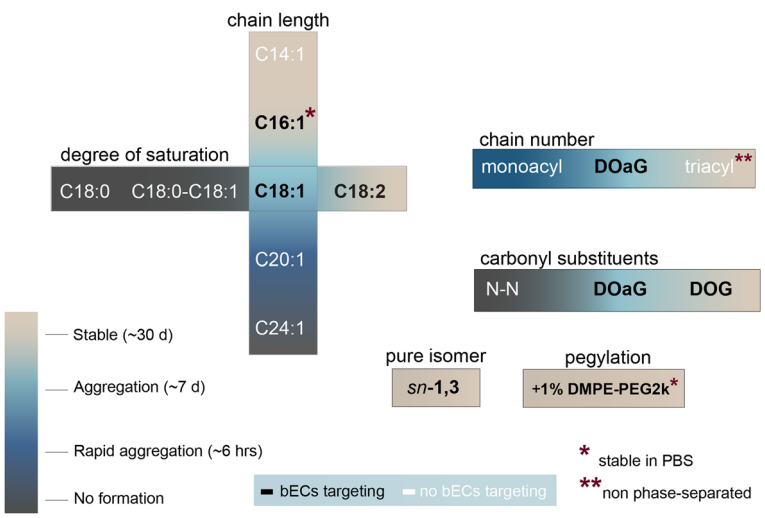

Fig. 6 Summary of DOaG analogues and the relationship between chemical character and stability, morphology and *in vivo* behavior of resulting liposomes. Stability: stable for ~30 days (beige), aggregation after ~7 days (light blue), rapid aggregation after ~6 hours (dark blue), no formation (dark grey). Analogues which result in liposomes targeting bECs are written in black letters and not targeting bECs in white letters. * Stable in PBS, **Non phase-separated.

Conclusion

Diacylglycerols are lipids that have unique properties in lipid membranes. From membrane alteration and phase transitions to signaling and protein recruitment, these lipids can be proven to be interesting lipid components in lipid-based nanoparticles. They could contribute to novel formulations with unique properties and functions, such as *in vivo* specificity, nanoparticle–protein communication, fusion and enhanced endosomal escape. It would be interesting to see whether newly developed lipid-based nanoparticles incorporating medium-chain, unsaturated DAG analogues can exhibit any of the above characteristics. Overall, the development of more effective and rationally designed nanomedicines requires a deeper understanding on how lipid composition affects morphology and biodistribution.

Methods

Liposome formulation

Liposomes were formulated by extrusion in ddH_2O at a total lipid concentration of 5 mM, except for the PBS studies for which they were formulated in PBS. Individual lipids as stock solutions (1–10 mM) in chloroform were combined to the desired molar ratios and dried to a thin film, first under a N_2 stream, then >1 h under vacuum. The fluorescent reporter DOPE-LR (1,2-dioleoyl-*sn-glycero*-3-phosphoethanolamine-*N*-(lissamine rhodamine B sulfonyl)) was also added in the lipid film at 0.2% moL. Lipid films were hydrated with 1 mL ddH_2O (or PBS) above the T_m of all lipids (65 °C), with gentle vortexing if necessary, to form a suspension. Large unilamellar vesicles were formed through extrusion (mini extruder, Avanti Polar Lipids) above the T_m of all lipids (*i.e.*, 65 °C). Hydrated lipids were passed 11 times through 2 × 400 nm polycarbonate (PC) membranes (Nucleopore Track-Etched membranes, Whatman), followed by 11 times through 2 × 100 nm PC membranes. All liposomes were freshly made for cryo-TEM imaging and intravenous administration in zebrafish embryos. Subsequently, all formulations were stored at 4 °C for a period of 30 days with their size and PDI measured occasionally.

Hydrodynamic diameter and PDI measurements

The hydrodynamic diameter and polydispersity index (PDI) of liposomes were obtained by using a Malvern Zetasizer Nano ZS. DLS measurements (operating wavelength = 633 nm) were carried out at room temperature in water at a total lipid concentration of approx. 100 μM. All reported DLS measurements are the average of three measurements.

Cryogenic transmission electron microscopy

Liposomes (3 μL, 5 mM total lipid concentration) were applied to a freshly glow-discharged carbon 200 mesh Cu grid (Lacey carbon film, Electron Microscopy Sciences, Aurion, Wageningen, The Netherlands). Grids were blotted for 3 s at 99% humidity in a Vitrobot plunge-freezer (FEI VitrobotTM Mark III, Thermo Fisher Scientific). For PAP3 liposomes imaged at 45 °C < T < 65 °C, liposomes were prepared by extrusion at 65 °C and immediately transferred in a thermomixer with a stable temperature of 65 °C, without allowing the liposomes to reach room temperature at all times. Subsequently, liposomes were transferred in the plunge-freezer operating at 45 °C and immediately vitrified. Cryo-TEM images were obtained on a Talos L120C (NeCEN, Leiden University) or a Titan KRIOS (TU Eindhoven) operating at 120 kV or 300 kV, respectively. Images acquired on the Talos microscope were recorded manually at a nominal magnification of 13500× or 22000× yielding a pixel size at the specimen of 7.44 or 4.40 ångström (Å), respectively. Images acquired on the KRIOS microscope were recorded manually at a nominal magnification of 6500× or 24000× yielding a pixel size at the specimen of 13.99 or 3.87 ångström (Å), respectively.

Zebrafish husbandry and injections

Zebrafish (*Danio rerio*, strain AB/TL) were maintained and handled according to the guidelines from the Zebrafish Model Organism Database (**https://zfin.org**) and in compliance with the directives of the local animal welfare committee of Leiden University. Fertilization was performed by natural spawning at the beginning of the light period, and eggs were raised at 28.5 °C in egg water (60 μg mL^{-1} Instant Ocean sea salts). The previously established zebrafish line Tg(*kdrl*:eGFP)^{s843} was used throughout this study.[41] Liposomes were injected into zebrafish embryos (78 hours post fertilization) using a modified microangiography protocol.[42] Embryos were anesthetized in 0.01% tricaine and embedded in 0.4% agarose containing tricaine before injection. To improve the reproducibility of microangiography experiments, 1 nL injection volume was calibrated before liposomes were injected into the sinus venosus/duct of Cuvier. A small injection space was created by penetrating the skin with the injection needle and gently pulling the needle back, thereby creating a small pyramidal space in which the liposomes were injected. Successfully injected embryos were identified through the backward translocation of venous erythrocytes and the absence of damage to the yolk ball. Injection in zebrafish embryos and imaging of biodistribution of each formulation were conducted more than once to obtain n > 1. Each time freshly made liposomes were prepared.

Confocal imaging acquisition and editing

Zebrafish embryos were randomly picked from a dish of 20–60 successfully injected embryos. Confocal *z*-stacks were captured on a Leica TCS SPE or SP8 confocal microscope, using a 10× air objective (HCX PL FLUOTAR), a 40× water-immersion objective (HCX APO L) or a 63× water-immersion objective (HC PL APO CS). For whole-embryo views, 3 overlapping *z*-stacks were captured to cover the complete embryo. Laser intensity, gain and offset settings were identical between stacks and experiments. Images were processed using the Fiji distribution of ImageJ. Confocal image stacks (raw data) are available upon request. Fig. 3 and 4 show fluorescent signals from DOPE-LR only (gray scale, excited at 552 nm and emission measured in

the range of 500–650 nm). Colocalization of DOPE-LR (liposomes) and eGFP (zebrafish) is shown in Fig. S4 and S9.†

Author contributions

P. P. and G. A. contributed equally to this project. A. K. and F. C. conceptualized the idea. P. P, G. A, and F. C. designed the experiments. P. P. designed the experiments of Fig. 5. P. P., G. A., P.W., T.P., N.v.K., T.S., D.A., W.v.O., and Y.Z. carried out the experiments. P.P. and G.A. analyzed the data. P.P. wrote the manuscript – original draft with feedback from all authors. A. K. reviewed and edited the manuscript. M.M. and N.S. carried out a part of the cryoEM imaging. A.K. supervised and funded the research.

Data availability

All data are available upon reasonable request.

Conflicts of interest

There are no conflicts to declare.

Acknowledgements

This work was supported by the 2017 Leiden/Huygens Scholarship grant (awarded to P. P.). This work benefited from access to the Netherlands Centre for Electron Nanoscopy (NeCEN) at Leiden University, an Instruct-ERIC centre, with technical assistance from Ludovic Renault, Willem Noteborn and Birgit Luef. As part of the COFUND project oLife, D. A. acknowledges funding from the European Union's Horizon 2020 research and innovation program under Grant Agreement 847675. We also would like to thank Roy Pattipeiluhu for fruitful discussions that helped realizing this project. We also thank Hans van den Elst for conducting the HR-MS measurements.

References

1 X. Duan and Y. Li, Physicochemical Characteristics of Nanoparticles Affect Circulation, Biodistribution, Cellular Internalization, and Trafficking, *Small*, 2013, **9**(9–10), 1521–1532.
2 M. J. Mitchell, M. M. Billingsley, R. M. Haley, M. E. Wechsler, N. A. Peppas and R. Langer, Engineering Precision Nanoparticles for Drug Delivery, *Nat. Rev. Drug Discovery*, 2020, **20**(2), 101–124.
3 E. Blanco, H. Shen and M. Ferrari, Principles of Nanoparticle Design for Overcoming Biological Barriers to Drug Delivery, *Nat. Biotechnol.*, 2015, **33**(9), 941–951.
4 M. Li, X. Jin, T. Liu, F. Fan, F. Gao, S. Chai and L. Yang, Nanoparticle Elasticity Affects Systemic Circulation Lifetime by Modulating Adsorption of Apolipoprotein A-I in Corona Formation, *Nat. Commun.*, 2022, **13**(1), 1–16.
5 R. Pattipeiluhu, G. Arias-Alpizar, G. Basha, K. Y. T. Chan, J. Bussmann, T. H. Sharp, M.-A. Moradi, N. Sommerdijk, E. N. Harris, P. R. Cullis, A. Kros, D. Witzigmann and F. Campbell, Anionic Lipid Nanoparticles Preferentially Deliver mRNA to the Hepatic Reticuloendothelial System, *Adv. Mater.*, 2022, **34**(16), 2201095.
6 F. Campbell, F. L. Bos, S. Sieber, G. Arias-Alpizar, B. E. Koch, J. Huwyler, A. Kros and J. Bussmann, Directing Nanoparticle Biodistribution through Evasion and Exploitation of Stab2-Dependent Nanoparticle Uptake, *ACS Nano*, 2018, **12**(3), 2138–2150.
7 G. Arias-Alpizar, B. Koch, N. M. Hamelmann, M. A. Neustrup, J. M. J. Paulusse, W. Jiskoot, A. Kros and J. Bussmann, Stabilin-1 Is Required for the Endothelial Clearance of Small Anionic Nanoparticles, *Nanomedicine*, 2021, **34**, 102395.
8 G. Arias-Alpizar, L. Kong, R. C. Vlieg, A. Rabe, P. Papadopoulou, M. S. Meijer, S. Bonnet, S. Vogel, J. van Noort, A. Kros and F. Campbell, Light-Triggered Switching of Liposome Surface Charge Directs Delivery of Membrane Impermeable Payloads in Vivo, *Nat. Commun.*, 2020, **11**(1), 1–14.
9 H. Ishiwata, N. Suzuki, S. Ando, H. Kikuchi and T. Kitagawa, Characteristics and Biodistribution of Cationic Liposomes and Their DNA Complexes, *J. Controlled Release*, 2000, **69**(1), 139–148.
10 E. C. Cho, J. Xie, P. A. Wurm and Y. Xia, Understanding the Role of Surface Charges in Cellular Adsorption versus Internalization by Selectively Removing Gold Nanoparticles on the Cell Surface with a I 2/KI Etchant, *Nano Lett.*, 2009, **9**(3), 1080–1084.
11 P. R. Cullis, M. J. Hope and C. P. S. Tilcock, Lipid Polymorphism and the Roles of Lipids in Membranes, *Chem. Phys. Lipids*, 1986, **40**(2–4), 127–144.
12 V. A. Frolov, A. V. Shnyrova and J. Zimmerberg, Lipid Polymorphisms and Membrane Shape, *Cold Spring Harbor Perspect. Biol.*, 2011, **3**(11), a004747.
13 I. M. Hafez and P. R. Cullis, Roles of Lipid Polymorphism in Intracellular Delivery, *Adv. Drug Delivery Rev.*, 2001, **47**(2–3), 139–148.
14 S. Patel, N. Ashwanikumar, E. Robinson, Y. Xia, C. Mihai, J. P. Griffith, S. Hou, A. A. Esposito, T. Ketova, K. Welsher, J. L. Joyal, Ö. Almarsson and G. Sahay, Naturally-Occurring Cholesterol Analogues in Lipid Nanoparticles Induce Polymorphic Shape and Enhance Intracellular Delivery of mRNA, *Nat. Commun.*, 2020, **11**(1), 1–13.
15 G. Arias-Alpizar, P. Papadopoulou, X. Rios, K. R. Pulagam, M. A. Moradi, R. Pattipeiluhu, J. Bussmann, N. Sommerdijk, J. Llop, A. Kros and F. Campbell, Phase-Separated Liposomes Hijack Endogenous Lipoprotein Transport and Metabolism Pathways to Target Subsets of Endothelial Cells In Vivo, *Adv. Healthc. Mater.*, 2023, **12**(10), e2202709.

16 P. Papadopoulou, R. van der Pol, N. van Hilten, W. L. van Os, R. Pattipeiluhu, G. Arias-Alpizar, R. A. Knol, W. Noteborn, M. A. Moradi, M. J. Ferraz, J. M. F. G. Aerts, N. Sommerdijk, F. Campbell, H. J. Risselada, G. J. A. Sevink and A. Kros, Phase-Separated Lipid-Based Nanoparticles: Selective Behavior at the Nano-Bio Interface, *Adv. Mater.*, 2024, **36**(6), 2310872.

17 P. A. Janmey and P. K. J. Kinnunen, Biophysical Properties of Lipids and Dynamic Membranes, *Trends Cell Biol.*, 2006, **16**(10), 538–546.

18 D. P. Siegel and R. M. Epand, The Mechanism of Lamellar-to-Inverted Hexagonal Phase Transitions in Phosphatidylethanolamine: Implications for Membrane Fusion Mechanisms, *Biophys. J.*, 1997, **73**(6), 3089–3111.

19 S. C. Semple, A. Akinc, J. Chen, A. P. Sandhu, B. L. Mui, C. K. Cho, D. W. Y. Sah, D. Stebbing, E. J. Crosley, E. Yaworski, I. M. Hafez, J. R. Dorkin, J. Qin, K. Lam, K. G. Rajeev, K. F. Wong, L. B. Jeffs, L. Nechev, M. L. Eisenhardt, M. Jayaraman, M. Kazem, M. A. Maier, M. Srinivasulu, M. J. Weinstein, Q. Chen, R. Alvarez, S. A. Barros, S. De, S. K. Klimuk, T. Borland, V. Kosovrasti, W. L. Cantley, Y. K. Tam, M. Manoharan, M. A. Ciufolini, M. A. Tracy, A. de Fougerolles, I. MacLachlan, P. R. Cullis, T. D. Madden and M. J. Hope, Rational Design of Cationic Lipids for siRNA Delivery, *Nat. Biotechnol.*, 2010, **28**(2), 172–176.

20 P. R. Cullis and M. J. Hope, Lipid Nanoparticle Systems for Enabling Gene Therapies, *Mol. Ther.*, 2017, **25**(7), 1467–1475.

21 Y. Huang and S. Gui, Factors Affecting the Structure of Lyotropic Liquid Crystals and the Correlation between Structure and Drug Diffusion, *RSC Adv.*, 2018, **13**, 6978.

22 M. Johnsson, Y. Lam, J. Barauskas and F. Tiberg, Aqueous Phase Behavior and Dispersed Nanoparticles of Diglycerol Monooleate/Glycerol Dioleate Mixtures, *Langmuir*, 2005, **21**(11), 5159–5165.

23 G. Popescu, J. Barauskas, T. Nylander and F. Tiberg, Liquid Crystalline Phases and Their Dispersions in Aqueous Mixtures of Glycerol Monooleate and Glyceryl Monooleyl Ether, *Langmuir*, 2007, **23**(2), 496–503.

24 M. Johnsson, J. Barauskas and F. Tiberg, Cubic Phases and Cubic Phase Dispersions in a Phospholipid-Based System, *J. Am. Chem. Soc.*, 2005, **127**, 1076–1077.

25 M. Rakotoarisoa, B. Angelov, S. Espinoza, K. Khakurel, T. Bizien, M. Drechsler and A. Angelova, Composition-Switchable Liquid Crystalline Nanostructures as Green Formulations of Curcumin and Fish Oil, *ACS Sustainable Chem. Eng.*, 2021, **9**(44), 14821–14835.

26 A. Angelova, B. Angelov, M. Drechsler, T. Bizien, Y. E. Gorshkova and Y. Deng, Plasmalogen-Based Liquid Crystalline Multiphase Structures Involving Docosapentaenoyl Derivatives Inspired by Biological Cubic Membranes, *Front. Cell Dev. Biol.*, 2021, **9**, 617984.

27 F. M. Goñi and A. Alonso, Structure and Functional Properties of Diacylglycerols in Membranes, *Prog. Lipid Res.*, 1999, **38**(1), 1–48.

28 P. Campomanes, V. Zoni and S. Vanni, Local Accumulation of Diacylglycerol Alters Membrane Properties Nonlinearly Due to Its Transbilayer Activity, *Commun. Chem.*, 2019, **2**(1), 1–8.

29 M. Alwarawrah, F. Hussain and J. Huang, Alteration of Lipid Membrane Structure and Dynamics by Diacylglycerols with Unsaturated Chains, *Biochim. Biophys. Acta, Biomembr.*, 2016, **1858**(2), 253–263.

30 E. M. Goldberg, D. S. Lester, D. B. Borchardt and R. Zidovetzki, Effects of Diacylglycerols on Conformation of Phosphatidylcholine Headgroups in Phosphatidylcholine/Phosphatidylserine Bilayers, *Biophys. J.*, 1995, **69**(3), 965–973.

31 M. Alwarawrah, J. Dai and J. Huang, Modification of Lipid Bilayer Structure by Diacylglycerol: A Comparative Study of Diacylglycerol and Cholesterol, *J. Chem. Theory Comput.*, 2012, **8**(2), 749–758.

32 E. M. Goldberg, D. S. Lester, D. B. Borchardt and R. Zidovetzki, Effects of Diacylglycerols and Ca2+ on Structure of Phosphatidylcholine/Phosphatidylserine Bilayers, *Biophys. J.*, 1994, **66**, 382–393.

33 R. M. C. Dawson, N. L. Hemington and R. F. Irvine, Diacylglycerol Potentiates Phospholipase Attack upon Phospholipid Bilayers: Possible Connection with Cell Stimulation, *Biochem. Biophys. Res. Commun.*, 1983, **117**(1), 196–201.

34 J. A. Szule, N. L. Fuller and P. R. Rand, The Effects of Acyl Chain Length and Saturation of Diacylglycerols and Phosphatidylcholines on Membrane Monolayer Curvature, *Biophys. J.*, 2002, **83**(2), 977–984.

35 M. N. Holme, M. H. Rashid, M. R. Thomas, H. M. G. Barriga, K. L. Herpoldt, R. K. Heenan, C. A. Dreiss, J. L. Bañuelos, H. N. Xie, I. Yarovsky and M. M. Stevens, Fate of Liposomes in the Presence of Phospholipase C and D: From Atomic to Supramolecular Lipid Arrangement, *ACS Cent. Sci.*, 2018, **4**(8), 1023–1030.

36 G. J. Strijkers, W. J. M. Mulder, R. B. van Heeswijk, P. M. Frederik, P. Bomans, P. C. M. M. Magusin, K. Nicolay, K. Nicolay, B. Nmr and P. Bomans, Relaxivity of Liposomal Paramagnetic MRI Contrast Agents, *MAGMA*, 2005, **18**, 186–192.

37 J. C. Gómez-Fernández and S. Corbalán-García, Diacylglycerols, Multivalent Membrane Modulators, *Chem. Phys. Lipids*, 2007, **148**, 1–25.

38 A. J. Da Silva Sanchez, K. Zhao, S. G. Huayamares, M. Z. C. Hatit, M. P. Lokugamage, D. Loughrey, C. Dobrowolski, S. Wang, H. Kim, K. Paunovska, Y. Kuzminich and J. E. Dahlman, Substituting Racemic Ionizable Lipids with Stereopure Ionizable Lipids Can Increase mRNA Delivery, *J. Controlled Release*, 2023, **353**, 270–277.

39 M. Z. C. Hatit, C. N. Dobrowolski, M. P. Lokugamage, D. Loughrey, H. Ni, C. Zurla, A. J. Da Silva Sanchez, A. Radmand, S. G. Huayamares, R. Zenhausern, K. Paunovska, H. E. Peck, J. Kim, M. Sato, J. I. Feldman, M. A. Rivera, A. Cristian, Y. T. Kim, P. J. Santangelo and

J. E. Dahlman, Nanoparticle Stereochemistry-Dependent Endocytic Processing Improves in Vivo mRNA Delivery, *Nat. Chem.*, 2023, **15**, 508–515.

40 S. J. Allison and J. Milner, Influence of Polyethylene Glycol Lipid Desorption Rates on Pharmacokinetics and Pharmacodynamics of siRNA Lipid Nanoparticles, *Mol. Ther.–Nucleic Acids*, 2013, **2**(12), e139.

41 S. W. Jin, D. Beis, T. Mitchell, J. N. Chen and D. Y. R. Stainier, Cellular and Molecular Analyses of Vascular Tube and Lumen Formation in Zebrafish, *Development*, 2005, **132**(23), 5199–5209.

42 G. Arias-Alpizar, J. Bussmann and F. Campbell, Zebrafish Embryos as a Predictive Animal Model to Study Nanoparticle Behavior in Vivo, *Bio-Protoc.*, 2021, **11**(19), e4173.